MOLECULAR AND CELLULAR BIOLOGY, May 2006, p. 3752–3763 Vol. 26, No. 10
0270-7306/06/$08.00+0 doi:10.1128/MCB.26.10.3752–3763.2006

Cells Expressing Murine *RAD52* Splice Variants Favor Sister Chromatid Repair†

Peter H. Thorpe,[1] Vanessa A. Marrero,[1] Margaret H. Savitzky,[1]§ Ivana Sunjevaric,[1] Tom C. Freeman,[2]‡ and Rodney Rothstein[1]*

Department of Genetics and Development, Columbia University Medical Center, 701 West 168th St., New York, New York 10032,[1] and Gene Expression Group, Sanger Centre, Wellcome Trust Genome Campus, Hinxton, Cambridge CB10 1SA, United Kingdom[2]

Received 11 July 2005/Returned for modification 2 February 2006/Accepted 24 February 2006

The *RAD52* gene is essential for homologous recombination in the yeast *Saccharomyces cerevisiae*. *RAD52* is the archetype in an epistasis group of genes essential for DNA damage repair. By catalyzing the replacement of replication protein A with Rad51 on single-stranded DNA, Rad52 likely promotes strand invasion of a double-stranded DNA molecule by single-stranded DNA. Although the sequence and in vitro functions of mammalian RAD52 are conserved with those of yeast, one difference is the presence of introns and consequent splicing of the mammalian *RAD52* pre-mRNA. We identified two novel splice variants from the *RAD52* gene that are expressed in adult mouse tissues. Expression of these splice variants in tissue culture cells elevates the frequency of recombination that uses a sister chromatid template. To characterize this dominant phenotype further, the *RAD52* gene from the yeast *Saccharomyces cerevisiae* was truncated to model the mammalian splice variants. The same dominant sister chromatid recombination phenotype seen in mammalian cells was also observed in yeast. Furthermore, repair from a homologous chromatid is reduced in yeast, implying that the choice of alternative repair pathways may be controlled by these variants. In addition, a dominant DNA repair defect induced by one of the variants in yeast is suppressed by overexpression of *RAD51*, suggesting that the Rad51-Rad52 interaction is impaired.

Homology-directed repair (HDR) allows cells to repair DNA double-strand breaks (DSBs) in an error-free way and is a key mechanism for maintaining genome integrity in all eukaryotes (11, 48, 52). *RAD52* is an essential gene for HDR in the yeast *Saccharomyces cerevisiae* (20, 30, 46). Identified as one member of an epistasis group of radiation-sensitive yeast mutants, *rad52* strains are defective in HDR, the major DSB repair pathway in yeast. *RAD52* is largely conserved throughout eukaryotes, and both the human and yeast Rad52 proteins stimulate the replacement of replication protein A with Rad51 on single-stranded DNA (4, 29, 39, 45). Additionally, Rad52 promotes DNA annealing and strand exchange between a DNA duplex and complementary single-stranded DNA (14, 21, 27). Three-dimensional structures of the N terminus of human RAD52 (hRAD52) reveal a multimeric ring containing a positively charged surface groove that has been suggested to bind single-stranded DNA (15, 40). Relative to the N terminus of Rad52, the C terminus is poorly conserved between homologs. The C terminus of Rad52 is essential for its interaction with Rad51, a bacterial RecA homolog (26, 37). Consistent with its ability to bind both itself and other DNA repair proteins, Rad52 forms discrete nuclear foci both spontaneously and in response to DNA damage, and these DNA repair centers are the sites of DSB repair (23–25, 32).

Although yeast *RAD52* plays a critical role in HDR, surprisingly, *RAD52* knockout mice are resistant to DNA damage (35). However, it is likely that mammalian RAD52 is important for DNA repair, as its activities are conserved with yeast Rad52; in addition, HDR in chicken cells requires RAD52 (5, 42). Furthermore, *RAD52* null mice have a defect in gene targeting (35), and loss of *RAD52* rescues the tumorigenic phenotype of *ATM*-deficient mice (50). An alternative explanation for the phenotype of the *RAD52* knockout mice is that the functions of yeast Rad52 are redundant in higher eukaryotes. Mammals have a number of other genes, such as *XRCC3* and *BRCA2*, that may encode complementary functions with yeast *RAD52* (9, 10, 38).

Another difference between the mammalian and yeast *RAD52* genes is the presence of introns. The open reading frames (ORFs) of both human and mouse *RAD52* are divided into 12 exons whose positions relative to the RAD52 open reading frame are conserved. Splice variants of *hRAD52* have been isolated from cDNA libraries derived from both brain and testes tissues, and the encoded protein variants were found to bind to DNA but not to wild-type hRAD52 in vitro (16).

Here we report the isolation of two new splice variants from adult mouse tissues. We show that these variant transcripts act as dominant alleles in both mammalian cells and the yeast *S. cerevisiae*. In both mammalian cells and yeast, the variants perturb HDR, specifically by elevating the frequency of sister chromosome repair. In yeast, both variants also decrease the frequency of repair from a homologous chromatid. Further-

* Corresponding author. Mailing address: Department of Genetics and Development, Columbia University Medical Center, HHSC 1608, 701 West 168th St., New York, NY 10032. Phone: (212) 305-1733. Fax: (212) 923-2090. E-mail: rothstein@cancercenter.columbia.edu.

† Supplemental material for this article may be found at http://mcb.asm.org/.

‡ Present address: Scottish Centre for Genomic Technology and Informatics, University of Edinburgh Medical School, Chancellor's Building, Edinburgh EH16 4SB, United Kingdom.

§ Present address: Thomas A. Edison High School, 165-65 84th Avenue, Jamaica, NY 11432.

more, for one variant in yeast, the defect in DNA repair is suppressed by overexpression of *RAD51*. These data show that the splice variants have the potential to alter the ratio of repair from the homologous to the sister chromosome, possibly by impairing the interaction of Rad52 with Rad51.

MATERIALS AND METHODS

RNA isolation and reverse transcription-PCR (RT-PCR). Whole-tissue samples were homogenized first by passing approximately 15 mg tissue several times through a 27-gauge needle in RNAlater buffer (Ambion) and then through a QIAshredder column (QIAGEN). RNA was purified from the resulting suspension without delay using the RNAeasy column purification system (QIAGEN). Three to 5 μg of RNA was used for cDNA synthesis using random hexamer primers, thus ensuring that the cDNA represents all the transcripts present in the tissue. Either the Superscript first-strand synthesis system for RT-PCR (Invitrogen) or first-strand cDNA synthesis kit for RT-PCR (Roche) was used for this cDNA synthesis. Approximately 10% of the resulting cDNA was used as a template for PCR using gene specific primers.

As a control for cDNA yield, primers were designed to amplify a 209-bp product spanning exons 5 to 8 from a spliced transcript of the murine glyceraldehyde 3-phoshate dehydrogenase gene (*GAPDH*). Each RT reaction includes a matched control that omits the reverse transcriptase enzyme to confirm that the subsequent PCR products are derived from cDNA and not from DNA contamination. *GAPDH* primers used for PCR were 5′ TGGAGCCAAAGCGGTC ATCA and 5′ GTGGCAGTGATGGCATGGAC. *RAD52* exon 1 to 7 primers were 5′ AGTCTCCATTCCTTCTGCGAG and 5′ ACAGTTTCCAAGTGCAT TCCC. *RAD52* exon 6 to 11 primers were 5′ GGAAGGAGGCTGTGACT GATG and 5′ GGTTCTGCTCTACACAAGGGC (all oligonucleotides were obtained from Sigma-Genosys). All PCR amplifications used the following protocol: 95°C for 5 min, followed by 30 cycles of 94°C for 30 s, 55°C for 30 s, and 72°C for 1 min. The resulting PCR products were separated by Tris-borate-EDTA (TBE)-agarose gel electrophoresis, and the gels were blotted overnight onto Hybond-N+ membrane (Amersham Biosciences). The DNA was cross-linked to the Hybond blots using UV irradiation (120 mJ/cm^2 using a Stratalinker; Stratagene). The blots were then prehybridized with 100 μg/ml salmon testes DNA in PerfectHyb Plus buffer (Sigma) at 48°C for 1 to 2 h. To synthesize radiolabeled oligonucleotide probes, 1,000 U of T4 polynucleotide kinase (Roche) was used to label 40 ng (~6 pmol) oligonucleotide with 25 μCi (~8 pmol) [γ-^{32}P]ATP (PerkinElmer Life Sciences). For *GAPDH* blots, the primer 5′ TCCTGCACCAACTGCTTA was labeled. For *RAD52* exons 1 to 7, 5′ GGAA GGAGGCTGTGACTGATG was labeled, and for *RAD52* exons 6 to 11, both 5′ ACAGTTTCCAAGTGCATTCCC and 5′ CAGCCTCAGAACTCCTCCAGG were labeled. The oligonucleotide probes were hybridized with the blots overnight at 48°C. Blots were washed several times in 4× SSC (1× SSC is 0.15 M NaCl plus 0.015 M sodium citrate), 0.1% sodium dodecyl sulfate at room temperature before autoradiograph images were obtained.

To sequence the RT-PCR products, the samples were reamplified with an additional 30 cycles of PCR, and the products were separated by TBE-agarose gel electrophoresis. The bands corresponding to novel transcripts were cut from the gels, and the DNA was purified using QIAquick columns (QIAGEN).

Polyribosome preparation. Approximately 10^7 mouse 3T3 cells were washed once with ice-cold phosphate-buffered saline (PBS) and then scraped from the dish in 200 μl ice-cold, diethyl pyrocarbonate (DEPC)-treated lysis buffer (10 mM HEPES, 300 mM KCl, 5 mM $MgCl_2$, 0.5% NP-40). The lysate was passed three times through a 27-gauge needle, and the nuclei were removed by centrifugation (13,000 rpm) for 5 min at 4°C. The supernatant was applied directly to the top of a 10-ml, 15 to 45% DEPC-treated sucrose gradient (prepared in 10 mM HEPES, 300 mM KCl, 5 mM $MgCl_2$) and centrifuged at 38,000 rpm for 90 min at 3°C. Fractions were collected from the bottom of the gradient, monitored with UV absorbance (280 nm), and placed into an equal volume of RNAlater (QIAGEN). RNA was purified from these fractions using RNAeasy reagents (QIAGEN), and RT-PCR was performed as described above.

Mammalian cell culture transfections. A plasmid, pRAD52(pWJ1456), containing the mouse *RAD52* gene under the control of a cytomegalovirus immediate-early promoter was based on pIRES-EGFP. Briefly, the *RAD52* sequence obtained from mouse embryonic cDNA libraries was subcloned as a 1.6-kb EcoRI DNA fragment from pWJ669 (3) into the EcoRI cloning site of pIRES-EGFP (BD Biosciences, Clontech). Subsequently, the enhanced green fluorescent protein (EGFP) gene was removed by deletion of a 1-kb XmnI-NotI restriction endonuclease fragment from this and all other pIRES-EGFP-derived vectors used in this study. The two variant plasmids, pRAD52Δexon4(pWJ1457) and pRAD52+intron8(pWJ1458), were created using the Quickchange mutatgenesis kit (Stratagene) to alter the *RAD52* sequence. Briefly, pRAD52Δexon4 is identical to pRAD52, except for the deletion of 94 bp corresponding to *RAD52* exon 4. pRAD52+intron8 is identical to pRAD52, except for the inclusion of 139 bp of mouse *RAD52* intron 8 (derived from the RT-PCR of mouse tissues described above). pCMV(pWJ1459), lacking the *RAD52* gene, is a control vector.

Chinese hamster ovary cells (CHO) cells were used to assay HDR. These cells contain a direct repeat of the GFP gene in which one repeat is full length but is inactivated by the inclusion of an I-SceI endonuclease target site. The second repeat lacks both the 5′ and 3′ ends of the gene. After cleavage with the I-SceI endonuclease, the resulting DSB can be repaired by gene replacement from the second GFP repeat either from the same or from a sister chromosome, resulting in a functional GFP allele (see Fig. 5A). The efficiency of repair is scored by fluorescence-activated cell sorting (FACS). The plasmid encoding the homing endonuclease I-SceI (pCAGGS-I-SceI) as well as the CHO and CHO-*XRCC3*$^{-/-}$ cell lines containing the DR-GFP reporter were kind gifts from Maria Jasin and Jeremy Stark, and their use has been described elsewhere (31). Cells were grown in serum-plus medium (Dulbecco's modified Eagle medium containing 10% newborn bovine serum, 4.5 g/liter glutamine, 4.5 g/liter glucose, 110 mg/liter sodium pyruvate, and 100 U/ml penicillin-streptomycin; all from Invitrogen-GibcoBRL) at 37°C, 6% CO_2. Cells were harvested from culture dishes after 2 to 10 min of incubation with trypsin-EDTA (Invitrogen) and then washed once in PBS. Cells (2×10^5) were plated on 60-mm tissue culture dishes and grown overnight in serum-plus medium. The following day the cells were transfected in OPTIMEM medium (Invitrogen) with 4 μg/dish plasmid DNA (2 μg of pI-SceI and 2 μg of experimental plasmid as indicated), using 4 μl/dish lipofectin (Invitrogen) following the manufacturer's instructions (this DNA:lipofectin ratio was determined to be optimal for expression of GFP from the pIRES-GFP vector). Transfection was carried out for 5 h, after which the medium was replaced with serum-plus medium. After 48 h, the cells were collected using trypsin-EDTA, washed twice in PBS, and resuspended in 200 to 600 μl PBS. FACS analysis was performed on the cells as previously described (49). Expression levels of I-SceI from the pI-SceI vector were assumed to be equivalent in each case. The expression of the mammalian variants was assessed by a parallel experiment in which CHO cells were transfected with plasmids equivalent to those described above but including the internal ribosomal entry site (IRES)-GFP sequence. This GFP sequence produces fluorescence signal in all cells that successfully take up and express the plasmid vector. FACS analysis of the resulting transfections allowed the measurement of the proportion of CHO cells transfected (GFP$^+$). For each of the four vectors (pIRES-GFP, pRAD52-IRES-GFP, pRAD52Δexon4-IRES-GFP, and pRAD52+intron8-IRES-GFP) the number of cells transfected was equivalent (Fig. SB in the supplemental material).

Mammalian cell synchronization. To obtain a synchronous culture of mouse 3T3 cells, the cells were grown to near confluence in 150-cm^2 tissue culture flasks and then arrested with 400 ng/ml (1.3 μM) nocodazole for 6 h. The mitotic cells were then collected by mitotic shake-off, which involves mechanical shaking of the flasks for 5 min. The pooled mitotic cells were collected by centrifugation, washed twice in nocodazole-free media, and then grown in nocodazole-free media. Cells were plated in 60-cm^2 dishes and harvested at various time points using trypsin. One aliquot was fixed in 100% ethanol at −20°C for at least 30 min. These fixed cells were then stained in PBS with 50 μg/ml propidium iodide and 200 μg/ml RNase A (Sigma) at 4°C for at least 30 min prior to FACS analysis. A second aliquot was placed directly into RLT buffer (QIAGEN) and stored at −80°C for RNA preparation as described above.

Yeast strains and methods. Standard genetic methods were used for the growth and manipulation of yeast (36). The yeast strains used in this study are listed in Table 1. The strains encoding Rad52 tagged with yellow fluorescent protein (YFP) and cyan fluorescent protein (CFP) have been reported previously (23). We modified W3749-14C (Rad52-YFP) using our previously published allele replacement method (8). Briefly, PCR primers were designed to generate targeting fragments that eliminate either the 3′ 1,281 bp of *RAD52* for *rad52Δ77-YFP* or the 3′ 660 bp of *RAD52* for *rad52Δ284*. The final five amino acids of yeast Rad52 encoded by *rad52Δ77* and *rad52Δ284* are -FGTSR and -DTDLK, respectively. The two resulting *RAD52* deletion strains (W5001-9C and W5002-5A) maintain the truncated yeast *RAD52* ORF in frame with the downstream YFP gene. The sensitivity of yeast strains to γ-irradiation was determined by growing strains in YPD to log phase and then plating on YPD plates and irradiating them using a Gammacell-220 ^{60}Co irradiator (Atomic Energy, Ottawa, Canada). The proportion of S/G_2-phase cells in log-phase culture containing Rad52-YFP and -CFP foci were determined using fluorescence microscopy as previously described (23, 25). The fluorescence of tagged Rad52 protein in individual cells was measured by reconstructing cells in three dimensions from fluorescent images

TABLE 1. Yeast strains used in this study

Strain[a]	Relevant genotype
W5933	*rad52*::*HIS5*/*RAD52-YFP*
W5934	*rad52*::*HIS5*/*rad52Δ77-YFP*
W5935	*rad52*::*HIS5*/*rad52Δ284-YFP*
W5936	*rad52*::*HIS5*/*rad52*::*HIS5*
W5937	*RAD52-CFP*/*RAD52-YFP*
W5938	*RAD52-CFP*/*rad52Δ77-YFP*
W5939	*RAD52-CFP*/*rad52Δ284-YFP*
W5957	*ade2-n*/*ade2-a RAD52*/*RAD52*
W5958	*ade2-n*/*ade2-a RAD52*/*rad52*::*HIS5*
W5959	*ade2-n*/*ade2-a RAD52*/*rad52Δ77-YFP*
W5960	*ade2-n*/*ade2-a RAD52*/*rad52Δ284-YFP*
W5977	*leu2ΔEcoRI*::*URA*::*leu2ΔBstEII*/*leu2ΔEcoRI*::*URA*::*leu2ΔBstEII RAD52*/*RAD52*
W5978	*leu2ΔEcoRI*::*URA*::*leu2ΔBstEII*/*leu2ΔEcoRI*::*URA*::*leu2ΔBstEII RAD52*/*rad52*::*HIS5*
W5979	*leu2ΔEcoRI*::*URA*::*leu2ΔBstEII*/*leu2ΔEcoRI*::*URA*::*leu2ΔBstEII RAD52*/*rad52Δ77-YFP*
W5980	*leu2ΔEcoRI*::*URA*::*leu2ΔBstEII*/*leu2ΔEcoRI*::*URA*::*leu2ΔBstEII RAD52*/*rad52Δ284-YFP*

[a] All strains in this study are *RAD5*$^+$ derivatives of W303 (47, 54). In addition to the genotype listed above, all strains are *MAT***a**/*MATα lys2Δ*/*LYS2 trp1-1*/*TRP1* and homozygous for *ADE2 can1-100 ura3-1 his3-11,15 leu2-3,112*, except where indicated. Strains W5933 through W5939 are also homozygous for *bar1*::*LEU2*; the other strains are *BAR1*$^+$. The *rad52*::*HIS5* allele is *rad52Δ*.

and quantifying the relative fluorescence using Volocity software (Improvision, Lexington, MA).

The strains encoding the two heteroalleles of *ADE2* were a kind gift from Lorraine Symington, and their use has been described elsewhere (12). The *ade2-n* allele contains a fill-in mutation of the 3′ NdeI restriction endonuclease target site of the yeast *ADE2* gene, and the *ade2-a* allele contains a fill-in mutation of the 5′ AatII site (2). The frequency of heteroallelic recombination was measured for at least nine independent isolates of each diploid strain. Cells were grown overnight in synthetic complete (SC) medium and washed once in H_2O before being briefly sonicated. Serial 10-fold dilutions were plated both on SC medium and in duplicate on adenine-deficient medium. Colonies were counted after 48 h, and the method of Lea and Coulson was used to estimate "m," the mean number of recombinants per culture (22).

The strains used for the direct-repeat assay contain two defective *LEU2* alleles separated by a *URA* gene and were derived from previously published strain W1470 (41). Strains for direct-repeat recombination were treated in the same way as those for heteroallelic recombination, except that the cells were plated on SC and, in duplicate, on leucine-deficient medium. This direct-repeat recombination assay also allows us to measure the frequency of single-strand annealing (SSA) events, which are scored by the loss of a *URA3* marker (pop-out), which is placed between the two repeated *leu2* alleles. As the *leu2* direct repeat is present as a diploid, *LEU2*$^+$ cells resulting from SSA events will be *ura3*$^-$/*URA3*$^+$, compared to *URA3*$^+$/*URA3*$^+$ for replacement events. Plating the *LEU2*$^+$ colonies on medium containing 5-fluoroorotic acid (5-FOA), which selects against *URA3*, allowed us to differentiate the *URA3* genotype. The colonies that were *ura3*$^-$/*URA3*$^+$, when replica plated to 5-FOA, produced small papillae, indicative of their ability to lose the single *URA3*$^+$ gene. In contrast, the *URA3*$^+$/*URA3*$^+$ colonies failed to grow at all on 5-FOA. Sporulating a selection of each class of *LEU*$^+$ colonies and testing the ability of the haploid spores to grow on uracil-deficient medium confirmed their *URA3* genotypes (data not shown). This allowed us to estimate the proportion of *LEU*$^+$ recombinants resulting in pop-out events compared to replacement events (illustrated in Fig. 6A).

RESULTS

Identification of mouse splice variants. Preliminary data derived from our sequencing of the mouse *RAD52* gene (unpublished observations) and from RT-PCR from an array of different mouse tissues (see Fig. SA in the supplemental material) suggested that at least two splice variants of mouse *RAD52* are commonly expressed. To investigate these findings further, tissue samples of lung and liver were dissected from two C57BL/6J mice and used for RT-PCR. A series of overlapping PCRs were performed covering the length of the mouse *RAD52* cDNA, as illustrated in Fig. 1A. The murine *RAD52* gene contains 12 exons. Three PCRs amplify cDNA from exons 1 to 7, 6 to 11, and 10 to 12. These PCRs were designed to detect most alterations in splicing that are pre-

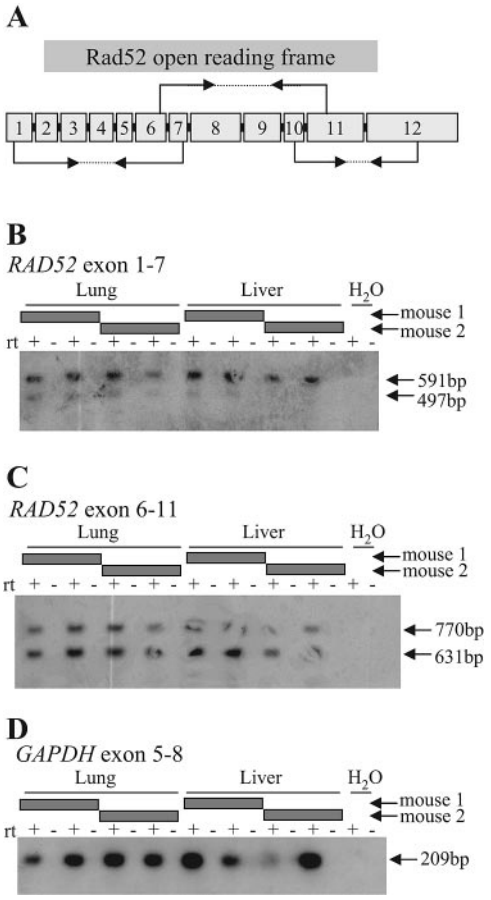

FIG. 1. (A) Twelve exons of the mouse *RAD52* gene are shown as numbered boxes approximately to scale; the position of each intron is shown as a short gap, but the introns are not shown to scale. A gray box above the gene indicates the open reading frame of the full-length RAD52 peptide, which extends from the start of exon 2 to the start of exon 12. The three primer pairs for RT-PCR across the *RAD52* transcript are indicated by converging arrows (exons 1 to 7, 6 to 11, and 10 to 12). (B, C, and D) Autoradiographs of the blots derived from the mouse RT-PCR are shown. A limited number of PCR cycles (30) was used, followed by genomic blotting, to ensure that all products detected are specific for the mouse *RAD52* gene. Each autoradiograph has 18 lanes, 8 with samples derived from the lung and 8 with samples derived from liver, plus 2 control lanes (H_2O, no template added). Two separate tissue samples were prepared from each of the two mice, and in each case the cDNA was prepared with and without reverse transcriptase (rt, indicated by + or − above the lanes) to ensure that all products are derived from RNA. The sizes of the bands are indicated based upon the position of size markers from the original TBE-agarose gels. The top autoradiograph (B) shows the results using primers designed to amplify *RAD52* exons 1 to 7, and the middle autoradiograph (C) shows the results using primers designed to amplify *RAD52* exons 6 to 11. The bottom autoradiograph (D) shows the results using primers designed to amplify *GAPDH* exons 5 to 8, which serves as a control for RNA preparation.

```
RAD52            1 MAGPEEAVHRGCDNHPPFVGGKSVLLFGQSQYTADEYQAIQKALRQRLGP  50
RAD52+intron8    1 MAGPEEAVHRGCDNHPPFVGGKSVLLFGQSQYTADEYQAIQKALRQRLGP  50
RAD52Δexon4      1 MAGPEEAVHRGCDNHPPFVGGKSVLLFGQSQYTADEYQAIQKALRQRLGP  50

RAD52           51 EYISSRMAGGGQKVCYIEGHRVINLANEMFGYNGWAHSITQQNVDFVDLN  100
RAD52+intron8   51 EYISSRMAGGGQKVCYIEGHRVINLANEMFGYNGWAHSITQQNVDFVDLN  100
RAD52Δexon4     51 EYISSRMAGGGQKILLTSTMASSTWESVHL                      80

RAD52          101 NGKFYVGVCA.....................................GAKDISSSCS  250
RAD52+intron8  101 NGKFYVGVCA.....................................GAKDISSSWY  250

RAD52          251 LAATLESDATHQRKLRKLRQKQLQQQFREQMETRRQSHAP...  290 of 420
RAD52+intron8  251 WAQVPLFLSGPFSCGFGQFPLLHLKPASGLCASSSRVHCG          290
```

FIG. 2. RAD52 peptide is aligned with the predicted product of the two variant transcripts, RAD52Δexon4 and RAD52+intron8. The RAD52Δexon4 sequence includes the first 63 amino acids of RAD52 followed by 18 "out of frame" amino acids (underlined and italicized), encoded by exon 5. The RAD52+intron8 sequence includes the first 248 amino acids of RAD52, followed by 42 amino acids encoded by intron 8 (underlined and italicized).

dicted from earlier studies (Fig. SA), such as the removal of exon sequence or the inclusion of intron sequences. Gels were blotted and probed with radiolabeled oligonucleotides to ensure that the RT-PCR products are specific for the *RAD52* gene. Using a relatively low number of PCR cycles and subsequent gel blotting also allows a semiquantitative assessment of the template RNA, as the RT-PCRs have not saturated.

We observed two variant products consistent with alternative splicing in addition to the expected *RAD52* transcript products corresponding to the annotated *RAD52* sequence (Fig. 1B and C). The expected product from exons 1 to 7 is 591 bp; however, a smaller, ~500-bp product was also identified (Fig. 1B). As depicted in Fig. 1C, products amplified from exons 6 to 11 give rise to a larger product of 750 to 800 bp in addition to the expected 631-bp product. No alternatively spliced products were observed from exons 10 to 12 (data not shown). Figure 1D shows the *GAPDH* control.

Both of these variant products are predicted to encode truncated RAD52 peptides (Fig. 2). DNA sequencing of the novel products revealed the alternative splicing. The small-variant product from exons 1 to 7 corresponds to a deletion of *RAD52* exon 4 (*RAD52Δexon4*). The sequence of the large-variant product from exons 6 to 11 corresponds to an inclusion of the intron 8 sequence (*RAD52+intron8*). *RAD52Δexon4* is predicted to encode amino acids 1 to 63 of RAD52 and 17 "out of frame" amino acids from exon 5. *RAD52+intron8* is predicted to encode amino acids 1 to 248 of RAD52, and 42 "novel" amino acids are encoded by intron 8.

Splice variants are associated with polyribosomes. The *RAD52* splice variants are predicted to encode C-terminal truncations of the RAD52 protein. Since degradation products of normal RAD52 could confound the results of a protein blot and specific antibodies to the N terminus of murine RAD52 are not available, we had to rely on additional evidence to determine if the splice variants are being translated. In particular, we searched for these splice-variant mRNAs on polyribosomes, the mRNA-ribosome complexes that are active in translation. Polyribosomes were purified from mouse 3T3 cells and fractionated based on size using 15% to 45% sucrose density gradients, which isolate polyribosomes containing four to six ribosomes in the middle of the gradient (the UV absorbance profile at 280 nm is provided in Fig. SC in the supplemental material). These fractions were then analyzed using the same splice-specific RT-PCR strategy used to originally identify the variants (described above) to screen for *RAD52Δexon4* and *RAD52+intron8*. The normal *RAD52* transcript and both of the splice variants are associated with polyribosomes (Fig. 3), indicating that the normal and variant *RAD52* transcripts are being actively translated in these mouse cells.

Splice variants are expressed uniformly throughout the cell cycle. Since Rad52 is thought to act primarily in S and G_2 and to be inactive in G_1, it is of interest to assay the expression of the splice variants throughout the cell cycle. Therefore, the expression of the variants in synchronized mouse 3T3 cells was examined as described in Materials and Methods. For each time point, an aliquot was stained with propidium iodide and used to analyze DNA content by FACS analysis, and a second aliquot was used for RNA preparation. RT-PCR was per-

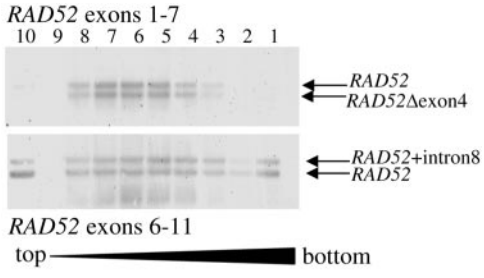

FIG. 3. Two autoradiographs are shown of blots of RT-PCRs specific for *RAD52Δexon4* (primers amplify exons 1 to 7, top) and *RAD52+intron8* (primers amplify exons 6 to 11, bottom). Each blot contains 10 lanes, representing the 10 fractions from the sucrose gradient, 1 to 10 in the order they came off the gradient. The lane to the right (1) represents products obtained from the bottom of the gradient; this may include some residual nuclei and high-molecular-mass complexes. The lanes to the left (8 to 10) contain low-molecular-mass complexes including free RNA molecules. Lanes 2 to 7 represent samples obtained from the polyribosome-containing fraction of the gradient. The UV absorbance profile of the polyribosome gradient is shown separately in Fig. SC of the supplemental material.

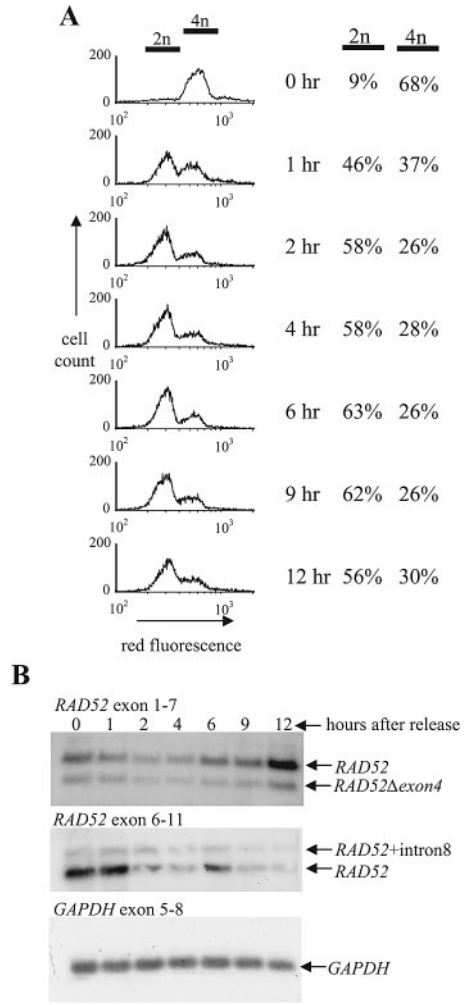

FIG. 4. (A) The FACS profile shows cells stained with propidium iodide at seven different time points after release from nocodazole arrest and mitotic shake off. At time zero the cells are arrested in G_2, by 6 h most of the cells have entered G_1, and by 12 h many of the cells have entered S phase. The percentages for 2n and 4n indicate the percentage of the cell population that fall within the limits of the black bars shown above the FACS profile. (B) Autoradiographs (as in Fig. 1B, C, and D) for the RT-PCR products used to identify *RAD52Δexon4* (top), *RAD52+intron8* (middle), and *GAPDH* control (bottom) from the time points shown above.

formed on the RNA as described above. Figure 4A shows the FACS profile of the cells following release from nocodazole arrest, and Fig. 4B shows the results of RT-PCR. We could detect no significant difference in the ratio of splice variant to normal transcript for either *RAD52Δexon4* or *RAD52+intron8* at any stage in the cell cycle. The RT-PCR products appear the same as asynchronously dividing cells (as in Fig. 3).

Splice variants modeled in mammalian cell culture cause dominant recombination effects. To test whether the mammalian splice variants cause functional changes in HDR, an established assay for gene repair in Chinese hamster ovary (CHO) cells was used. These cells contain the HDR reporter system outlined in Materials and Methods (also see Fig. 5A). Briefly, an I-SceI-induced DSB, within a nonfunctional GFP gene, can be repaired by gene conversion from a neighboring sequence to restore a functional GFP open reading frame. CHO cells were transfected with vectors expressing the normal *RAD52* cDNA, the two variant cDNAs, RAD52Δexon4 and RAD52+*intron8*, or the control (summarized in Fig. 5B). Expression of *RAD52* has no significant effect on HDR in this assay (Fig. 5C), similar to the expression of *RAD52* in a cell line mutated in *rad52* (43). Interestingly, expression of either of the splice variant constructs elevates the frequency of repair compared to that of full-length RAD52 (Fig. 5C).

Since there is evidence from chicken cells to suggest that *RAD52* acts in parallel with *XRCC3* in DNA damage repair (10), the mammalian HDR experiments were repeated with a CHO cell line that lacks *XRCC3* (CHO-*XRCC3*$^{-/-}$) to see how the splice variants act in this mutant. Consistent with previous observations (31), the overall frequency of HDR in this cell line is more than 10-fold lower than in wild-type cells. However, overexpression of the *RAD52* splice variants did not change the levels of HDR (Fig. 5D).

Finally, we attempted to knock down the level of the *RAD52+intron8* variant in CHO cells by designing small interfering RNA against the hamster intron 8 sequence. However, transfection of this small interfering RNA had no detectable effect on the level of the intron 8 variant (as judged by RT-PCR) or the frequency of recombination of the GFP targets in the presence of I-SceI (data not shown).

Splice variants modeled in yeast cause dominant recombination effects. The ability to conduct functional recombination studies in mammalian cells is currently hindered by the limited number of functional assays that distinguish between recombination products; for example, if it is difficult to differentiate repair from a homolog as opposed to a sister chromosome. Consequently, we employed the budding yeast *Saccharomyces cerevisiae* to assay for dominant-negative behavior of the splice variants. To mimic the C-terminal truncations that are predicted to be encoded by the two mouse splice variants, *RAD52Δexon4* and *RAD52+intron8*, the *RAD52-YFP* (encoding Rad52 fused to yellow fluorescent protein) gene from *Saccharomyces cerevisiae* (23) was modified at the yeast chromosomal locus. The *RAD52Δexon4* and *RAD52+intron8* mouse splice variants were recreated in the yeast *RAD52-YFP* gene as *rad52Δ77* and *rad52Δ284*, respectively (the numbers correspond to the final amino acid in the deleted Rad52 sequences). It is important to note that the mouse sequences were not transferred into yeast; rather, the yeast sequence was used to model the mouse transcripts by creating truncations of the endogenous yeast *RAD52* gene. We refer to these two yeast alleles as "splice variant equivalents."

As the mouse variants showed increased HDR when expressed in mammalian cells (Fig. 5), a similar repair assay was performed in yeast. Recombination between direct repeats was assayed using a reporter system containing two defective alleles of *LEU2* (*leu2ΔEcoRI* and *leu2ΔBstEII*) (Fig. 6A). Similar to the HDR assay used in CHO cells, the *leu2* direct-repeat reporter assays primarily intrachromatid and sister chromatid recombination (17, 41). Commonly, two kinds of *LEU2*$^+$ products result: replacements, where one of the *leu2* alleles is repaired without loss of the intervening *URA3* sequence; or pop-out events, where the *URA3* is lost by deletion of the sequence between the two *LEU2* alleles (Fig. 6A). As described in Materials and Methods, these two events are distinguished by a

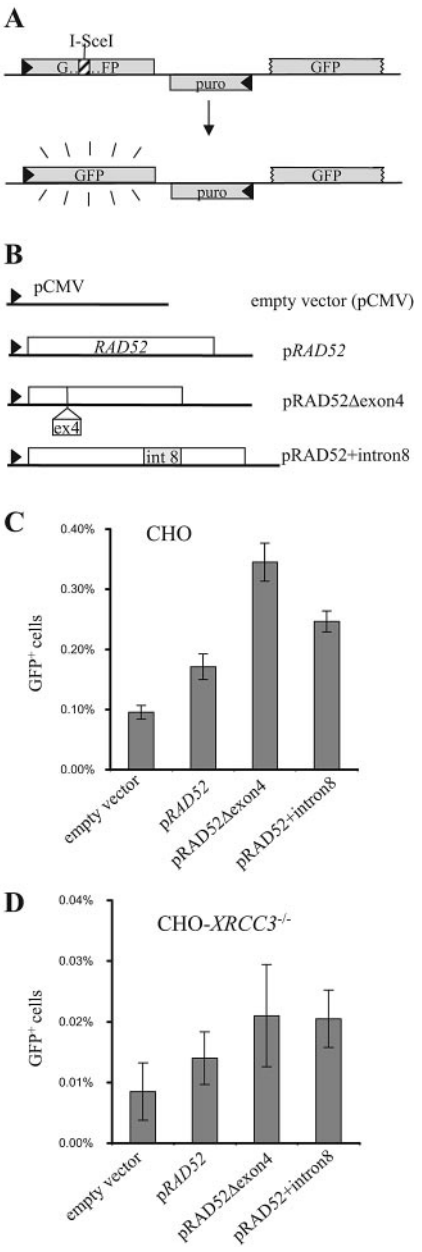

FIG. 5. (A) Schematic representation of the reporter system developed by Pierce and colleagues (31). puro, puromycin-*N*-acetyltransferase gene. A double-strand break can be introduced into this reporter using the I-SceI endonuclease, and subsequent HDR from a downstream GFP fragment enables the repair of a functional GFP sequence. These HDR events can be scored by FACS analysis. Four expression vectors were created from a derivative of the pIRES-EGFP vector (Clontech) as described in Materials and Methods (B). The four vectors include the empty vector control pCMV, full-length mouse *RAD52* (pRAD52), or the two splice variants, pRAD52Δexon4 and pRAD52+intron8, as indicated in panel B. (C) The frequency of HDR events in CHO cells (scored as % GFP^+ cells using FACS analysis) is shown. For each transfection the plasmid is indicated below. In addition, each transfection included an I-SceI-expressing plasmid; the mean of four experiments is indicated (±standard deviation). Analysis of variance indicates significant differences between the groups (data not shown). Both of the variant plasmids (pRAD52Δexon4 and pRAD52+intron8) have a higher frequency of HDR events than the wild-type *RAD52* plasmid (one-tailed *t* test, $P = 4.9 \times 10^{-5}$ and $P = 7.5 \times 10^{-4}$, respectively). A CHO cell line, deficient in *XRCC3*, was also tested in the same way (D). The difference between the wild-type *RAD52* plasmid and the pRAD52Δexon4 plasmid is not significant (one-tailed *t* test, $P = 0.094$). The difference between the wild-type *RAD52* plasmid and the pRAD52+intron8 plasmid is significant (one-tailed *t* test, $P = 0.044$).

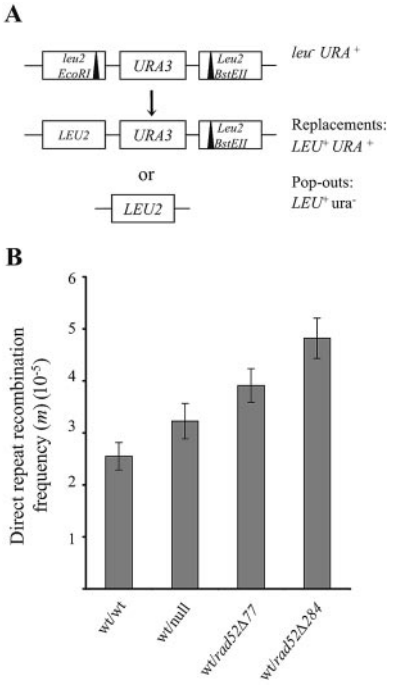

FIG. 6. (A) Frequency of direct-repeat recombination was assayed as indicated. Two *leu2* alleles are schematically represented (top), with dark triangles indicating the two mutations that inactivate the gene. Recombination between the two repeated sequences can restore a functional *LEU2* gene, and two possible LEU^+ recombinant structures are shown. First, a replacement event restores the wild-type *LEU2* sequence to one of the *leu2* alleles (e.g., the upstream sequence is restored). Second, a pop-out event is shown where single-strand annealing recombines the two repeated *leu2* alleles, leading to loss of the *URA3* gene and both mutations within *LEU2*. Other possible events such as triplications are discussed elsewhere (41). (B) The median *leu2* recombination frequency *m*, as defined by Lea and Coulson (22), is shown, where the error bars indicate ± standard deviation of *m*. The wild-type *RAD52* allele is abbreviated wt. Both variant alleles (*rad52Δ77*/null and *rad52Δ284*/null) have a higher frequency of direct-repeat recombination than the heterozygous wild-type strain (wt/null), (one-tailed *t* tests, $P = 8.5 \times 10^{-3}$ and 4.4×10^{-6}, respectively). The frequency of recombination in the heterozygous wild-type strain (wt/null) versus a wild-type diploid strain (wt/wt) is not significantly different (one-tailed *t* test, $P = 0.41$). Similarly, the recombination frequency in the *rad52Δ77*/null strain is not significantly different from that of the *rad52Δ284*/null strain (one-tailed *t* test, $P = 0.089$).

simple replica-plating assay. Since the mouse splice variants detected in our screen are expressed together with the normal transcript (Fig. 1B and C, 3, and 4B), we next created diploid yeast strains that contain a full-length *RAD52* allele in addition to a splice variant-equivalent allele to screen for dominant effects on direct-repeat recombination. Both of the *RAD52* splice variant equivalents elevate the frequency of $LEU2^+$ recombinants (Fig. 6B). While the effects upon recombination

TABLE 2. Proportion of replacements versus pop-outs from the direct-repeat recombination assay

Strain[a]	*RAD52* genotype	n^b	Proportion of *LEU2*$^+$ colonies that are *ura3*$^-$/*URA3*$^+$	Frequency of replacement events (10^{-5})[c]	Frequency of pop-out events (10^{-5})[c]
W5977	wt/wt	933	0.17	2.1	0.43
W5978	wt/*rad52*::*HIS5*	532	0.32	2.2	1.0
W5979	wt/*rad52Δ77-YFP*	1291	0.30	2.7	1.2
W5980	wt/*rad52Δ284-YFP*	1132	0.53	2.3	2.5

[a] wt, wild-type *RAD52* genotype. The full genotypes are listed in Table 1.
[b] *n* is the number of *LEU2*$^+$ colonies screened on 5-FOA-containing medium.
[c] The estimated frequencies of replacements and pop-outs are calculated using the total recombination frequencies, shown in Fig. 6B, adjusted by the proportions shown in this table.

are modest, they are significantly different from those of a heterozygous strain (one-tailed *t* tests, $P = 8.5 \times 10^{-3}$ and 4.4×10^{-6} for *rad52Δ77* and *rad52Δ284*, respectively). These effects are similar to those seen in mammalian cell culture (Fig. 5). Interestingly, in yeast, the *rad52Δ77* allele increases replacement events, while the *rad52Δ284* allele increases the frequency of *URA3* pop-outs (Table 2).

The yeast system has the advantage that the variants are easily assayed for effects on other types of DNA repair. Therefore, we analyzed the splice variant equivalents for their effects on heteroallelic recombination, focus formation, and DNA damage sensitivity. First, spontaneous heteroallelic recombination was assayed in diploid yeast with two defective *ade2* heteroalleles (*ade2-n* and *ade2-a*). Recombination between these alleles, which reside at each end of the *ADE2* gene on homologous chromatids, restores a functional *ADE2* gene (Fig. 7A). Surprisingly, in contrast to the elevated frequency of direct-repeat recombination seen in both mammalian cells (Fig. 5) and yeast (Fig. 6B), both of the splice variant equivalents lowered the frequency of yeast heteroallelic recombination (Fig. 7B). These disparate phenotypes suggest that the variants may be promoting sister chromatid repair while at the same time suppressing repair from a homologous chromosome.

In yeast, Rad52 and other DNA repair proteins form distinct nuclear foci at the sites of double-strand break repair (23–25). These DNA repair centers appear predominantly in S and G_2 phases of the cell cycle. Altered levels of foci within yeast strains are indicative of DNA repair deficiencies (25). Next, the formation of foci in the splice variant equivalent strains was measured using fluorescence microscopy. Both splice variant equivalents fail to form spontaneous foci in a haploid strain (data not shown). Diploid strains containing the splice variant equivalents tagged with YFP and wild-type Rad52 tagged with CFP (cyan fluorescent protein) were assayed for focus formation. Interestingly, in these strains, the Rad52Δ284-YFP protein forms foci that also contain wild-type Rad52-CFP (Fig. 8A), suggesting that Rad52Δ284-YFP and wild-type Rad52 are incorporated into the same DNA repair complex. The same phenotype is not observed for Rad52Δ77-YFP. Additionally, both splice variant equivalents elevate the proportion of S/G_2 cells that contain spontaneous wild-type Rad52 foci, indicative of either increased DNA damage or an altered DNA repair activity within these cells (Fig. 8B).

Unlike in mammalian cells, *RAD52* is essential for HDR in yeast, and furthermore HDR is its major DSB repair pathway. Therefore, DNA damage sensitivity is a standard assay for the function of yeast Rad52. First, we estimated protein levels in diploid strains containing differentially tagged Rad52 peptides (CFP and YFP) to ensure that the splice variant equivalent alleles do not alter the expression of *RAD52* from either the wild-type or mutant allele. Table 3 shows the amount of the YFP and CFP detected in the nucleus of the different strains, and there is no significant difference between the two mutant strains and the wild-type diploid. Next, the repair capacity of the splice variant equivalent strains was assayed by measuring viability with increasing doses of γ-irradiation. Both *rad52Δ77* and *rad52Δ284* are as sensitive to γ-irradiation as *rad52* null strains, either as haploid strains (data not shown) or as heterozygous diploids containing a null allele (Fig. 9A, first four rows). The diploid strains containing both a mutant and wild-type *RAD52* allele were tested for sensitivity to γ-irradiation, and *rad52Δ77* (Fig. 9A, sixth row) is as sensitive as a wild type/null (Fig. 9A, top row). In contrast, *rad52Δ284* confers a dominant-negative phenotype for γ-irradiation sensitivity (Fig. 9A, last row, indicated by the white arrow).

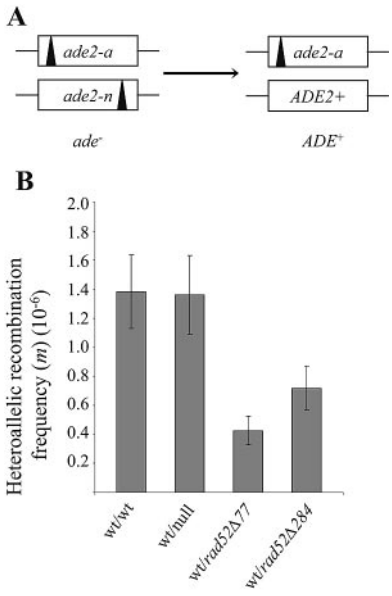

FIG. 7. (A) Heteroallelic recombination is measured using two *ade2* alleles as shown schematically. The dark triangles indicate the two mutations that inactivate the gene: *ade2-a* is a fill-in mutation of the AatII site in the 5′ end of the gene, and *ade2-n* is a fill-in mutation of the NdeI site in the 3′ end of the gene (12). Recombination between the two homologs restores a functional *ADE2* gene, as indicated. The gene conversion event depicted has lost the 3′ *ade2-n* mutation, leading to restoration of a functional *ADE2* gene. The frequency of heteroallelic recombination is calculated using the methods described by Lea and Coulson (22). (B) The median *ade2* recombination frequency *m* as defined by Lea and Coulson; the error bars indicate ± standard deviation of *m*. The wild-type allele is abbreviated wt. Both variant alleles (*rad52Δ77*/null and *rad52Δ284*/null) have a lower frequency of heteroallelic recombination than the heterozygous wild-type strain (wt/null) (one-tailed *t* tests, $P < 10^{-4}$). The frequency of recombination in the diploid wild-type strain (wt/wt) does not differ significantly from the heterozygous wild-type strain (wt/null) (two-tailed *t* test, $P = 0.87$). The *rad52Δ77*/null strain has a significantly lower frequency of recombination than the *rad52Δ284*/null strain (one-tailed *t* test, $P < 2 \times 10^{-4}$).

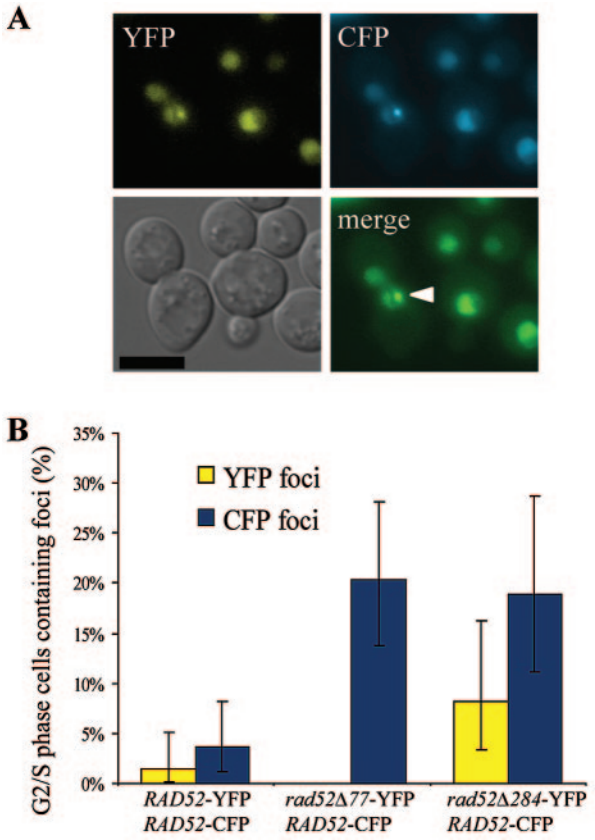

FIG. 8. (A) Microscopy of a diploid yeast strain containing both Rad52Δ284-YFP and Rad52-CFP, indicating colocalization. A spontaneously occurring Rad52 focus is seen in one cell, and both the YFP and CFP signals colocalize, as seen in the merged fluorescence image, indicated by a white arrowhead. The length of the scale bar in the bottom left of the bright-field image represents 5 μm. (B) The proportion of S/G_2-phase yeast cells (defined as mononuclear cells with a bud) that contain at least one Rad52 foci was calculated. The yellow bars indicate the proportion of cells with Rad52-YFP foci, and the blue bars indicate the proportion of cells with Rad52-CFP foci (CFP foci are brighter and more easily counted by microscopy, hence the higher proportion of CFP foci in the wild-type strain). The error bars indicate the 95% confidence intervals of the binomial proportions. The two diploid strains, containing novel variant alleles (*rad52Δ77-YFP/RAD52-CFP* and *rad52Δ284-YFP/RAD52-CFP*), have a significantly higher proportion of wild-type (CFP) foci than the wild-type diploid strain (*RAD52-YFP/RAD52-CFP*) (Fishers exact test, $P = 1.3 \times 10^{-5}$ and 2.3×10^{-4}, respectively).

Rad52 recruits Rad51 to sites of DNA damage and stimulates Rad51-mediated DNA strand exchange in vitro. Furthermore, overexpression of *RAD51* suppresses the phenotype of a Rad52 C-terminal truncation (1, 26). Therefore, we tested whether overexpression of the *RAD51* gene could rescue the dominant-negative γ-irradiation phenotype seen for *rad52Δ284.* The seven yeast strains shown in Fig. 9A were transformed with a plasmid containing the yeast *RAD51* gene under the control of a galactose-inducible promoter (pYES-S10-51; a kind gift from Thomas Kodadek). This plasmid complements a *rad51* null strain in the presence of galactose (data not shown). Figure 9B shows that the dominant-negative phenotype of *rad52Δ284* is partially rescued after induction of *RAD51* expression (compare the bottom rows of Fig. 9B, as indicated with a white arrow). This suggests that the radiation-sensitive phenotype of *rad52Δ284* is dependent on its disruption of Rad51 function(s).

DISCUSSION

Identification of novel *RAD52* transcripts from adult mouse tissue. Here we identify two novel *RAD52* transcripts from adult mouse tissue which are the major alternatively spliced mRNAs from this gene (Fig. 1). One variant aberrantly splices the *RAD52* mRNA from exon 3 directly to exon 5, skipping exon 4 (*RAD52Δexon4*), while the other variant fails to remove the short intron 8 (*RAD52+intron8*). These two variant mRNAs are predicted to encode truncations of the RAD52 peptide and are likely translated in vivo, since both are found on polyribosomes in the cytoplasm of mouse cells (Fig. 3). Furthermore, a *RAD52* IMAGE clone sequence was identified that lacks exon 4 (locus id:BC010673, gi:14715025), and sequences including *RAD52* intron 8 were identified from the National Center for Biotechnology Information Mouse Unigene Clusters Map (data not shown). However, definitive identification of these variants using database screening fails, because many cDNA clone sequences are derived from partially spliced transcripts. In addition, examination of the sequences at the intron-exon boundaries of murine *RAD52* does not identify deviations from the canonical splice sites to account for the alternate splicing. Thus, a solely bioinformatics approach is inadequate for identifying these novel splice variants, which requires the rigor of the RT-PCR analysis described here.

Testing the recombination phenotype of variant *RAD52* transcripts in cell culture. *RAD52Δexon4* and *RAD52+intron8* are predicted to encode truncated mouse RAD52 peptides of 80 and 290 amino acids, respectively (Fig. 2). We next tested the effects of the mouse variants on HDR in mammalian cells using direct repeats of GFP (Fig. 5A). Expression of the murine *RAD52* variants increase the frequency of gene replacement compared to wild-type mouse *RAD52* (Fig. 5), establishing that these variants are capable of altering the DNA repair phenotype of mammalian cells. Although the increase in HDR is small, it is consistent with the relatively modest effect on this type of assay seen when complementing *rad52* null cells (43). Several years ago, Kito et al. speculated that human *RAD52* splice variants similar in size to the mouse *RAD52Δexon4* transcript might confer a dominant-negative phenotype (16). Here we demonstrate that C-terminal truncations of RAD52 do in

TABLE 3. Quantification of Rad52 protein levels

Strain	*RAD52* genotype[a]	*n*	Quantification of CFP signal mean fluorescence[b]	Quantification of YFP signal mean fluorescence[b]
W5937	*RAD52-CFP/RAD52-YFP*	54	477.5 (±71)	257.2 (±12.5)
W5938	*RAD52-CFP/rad52Δ77-YFP*	47	504.6 (±40.7)	239.04 (±2.9)
W5939	*RAD52-CFP/rad52Δ284-YFP*	62	454.4 (±39.9)	264 (±12.5)

[a] The full genotypes are listed in Table 1. *n* indicates the number of cells measured for fluorescence. The amount of CFP is greater than YFP in all cases, as CFP gives a brighter fluorescence signal. It should be noted that nuclear fluorescence was measured in all cases, as Rad52 is localized within the nucleus. However, Rad52Δ77-YFP is localized throughout the cell.

[b] The mean fluorescence intensity (±standard deviation of the mean) is given in relative units.

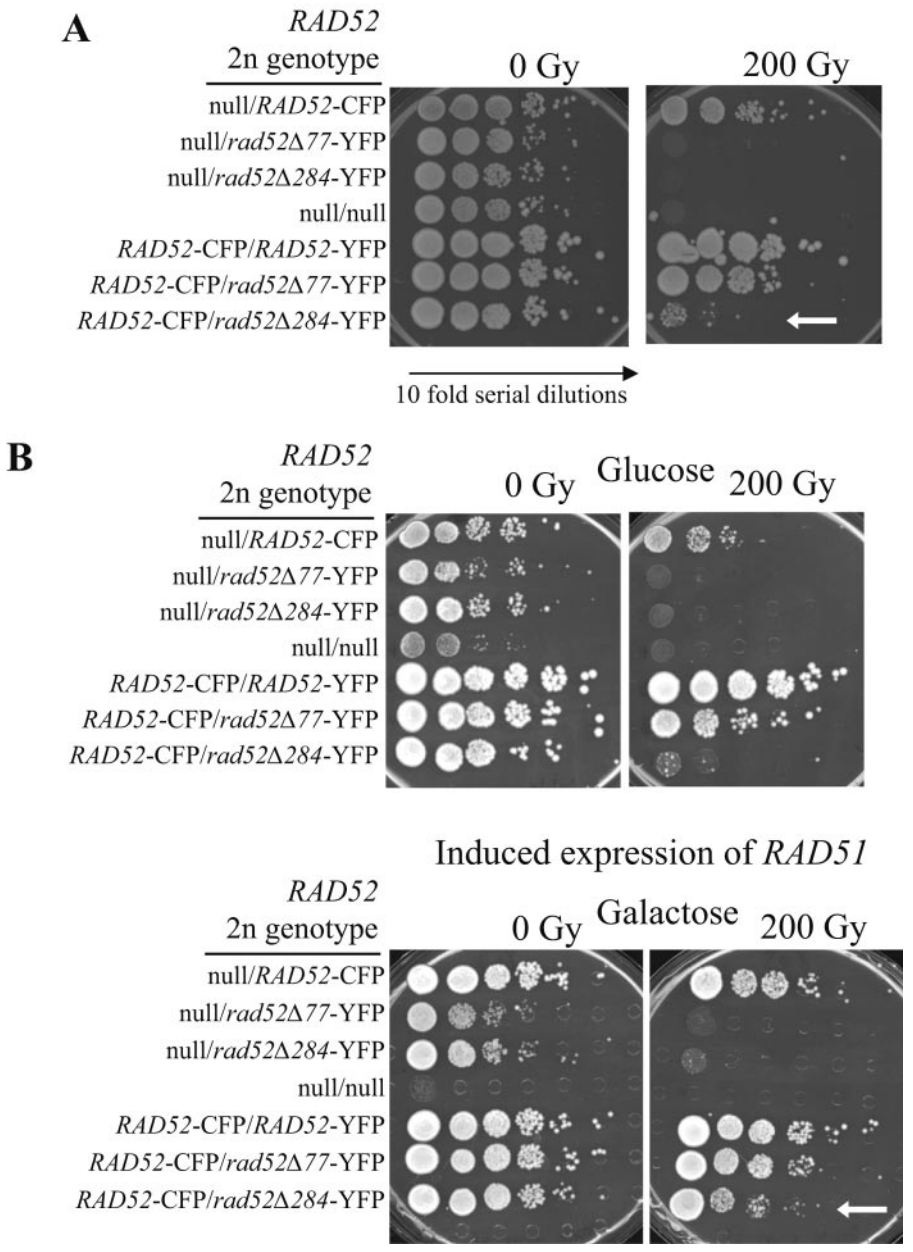

FIG. 9. (A) Two plates of yeast cultures are shown. On each plate seven strains are represented from top to bottom, and six successive 10-fold dilutions of each strain are plated from left to right. Two plates for each experiment were seeded identically, and one plate was exposed to 200 Gy of γ-irradiation. The white arrow at the bottom of the irradiated plate shows increased sensitivity for the heterozygous *rad52Δ284/RAD52* diploid strain compared to the top strain (wild-type/null), indicating the dominant-negative phenotype of *rad52Δ284*. The strains in both the top and bottom of panel B are the same as those described in panel A, except that they each contain plasmid pYES-S10-51 that expresses *RAD51* under the control of a galactose-inducible promoter. The top portion of panel B shows cells grown in the presence of glucose, which does not allow expression of *RAD51*. The lower portion of panel B shows galactose-induced cells expressing *RAD51*. Partial suppression of the γ-ray sensitivity of the *RAD52-CFP/rad52Δ284-YFP* strain, when grown on galactose, is indicated with a white arrow.

fact confer a dominant phenotype in mammalian cells by increasing recombination.

Testing the recombination phenotype of variant *RAD52* transcripts in yeast. The recombination assays available in mammalian cells have a number of limitations. We therefore modeled the splice variants in yeast to allow a further assessment of their role in DNA repair and recombination. A key advantage of modeling the mouse splice variants in yeast is that a range of well-characterized assays are available against which other defined alleles of Sc*Rad52* have previously been tested. Furthermore, the HDR assays available in yeast are more diverse and informative than the current mammalian assays.

The two mouse variants, *RAD52Δexon4* and *RAD52+intron8*, were modeled in the Sc*Rad52* gene (*rad52Δ77* and *rad52Δ284*, respectively). These alleles are referred to as "splice variant equivalents," since they truncate the yeast Rad52 protein at po-

sitions homologous to the mouse variants. The mammalian assay suggests that expression of the mouse variants elevates repair from the same or a sister chromosome (Fig. 5), therefore an equivalent yeast assay was performed. Direct-repeat recombination in yeast (Fig. 6) shows results similar to those seen in mammalian cells (Fig. 5), suggesting that the yeast splice variant equivalents do indeed model their mammalian counterparts. The splice variant equivalents show additional functional differences, which were revealed by further analysis of the *LEU2*$^+$ recombination products from the *leu2* direct-repeat assay. For *rad52Δ77*, the increased recombination is due to a modest increase in replacement events, whereas for *rad52Δ284* the increase is due to pop-out events (Table 2). In contrast to the increase in *leu2* direct-repeat recombination, the splice variant equivalents dominantly decrease the frequency of recombination between *ade2* heteroalleles (Fig. 7). These opposing recombination phenotypes suggest that the variants may bias the HDR pathway away from a homologous template toward a sister or intrachromatid template.

To probe further the dominant effects of the two splice variant equivalents, DNA damage sensitivity was tested. While mammalian *rad52* mutant cells exhibit limited DNA damage sensitivity, yeast *rad52* strains are exquisitely sensitive to DNA damage. Thus, in yeast, sensitivity to DNA damage provides a simple assay for *RAD52* function. As haploid cells, both *rad52Δ77* and *rad52Δ284* are sensitive to γ-irradiation (data not shown). These results were not surprising, since previous studies showed that truncations removing more than ~200 C-terminal amino acids of Sc*Rad52* render strains as sensitive as a *rad52* null strain to methyl methanesulfonate (MMS), a DNA-damaging agent (1, 6). In addition, a deletion of the last 175 codons of Sc*RAD52* confers a defective DSB repair phenotype (51).

Since the mammalian variants are coexpressed with full-length transcripts (Fig. 1B, C, 3, and 4B), diploid strains containing a splice variant equivalent allele and a wild-type Sc*RAD52* allele were tested for γ-ray sensitivity. The *Rad52Δ284* allele is dominant negative, while the *Rad52Δ77* allele is not (Fig. 9A). Previous work has shown that overexpression of two Sc*Rad52* C-terminal truncations confers a dominant-negative phenotype for sensitivity to MMS (26), suggesting that N-terminal Rad52 peptides are capable of disrupting the DNA repair ability of the full-length protein. Interestingly, structural analysis of both the full-length human RAD52 protein and an N-terminal fragment reveals a multimeric complex with RAD52 monomers arranged in a ring configuration (15, 40, 44). Therefore, it is likely that the RAD52+intron8 variant is incorporated into the ring and disrupts its function. This view is supported by our finding that Rad52Δ284 and wild-type Rad52 colocalize in foci (Fig. 8A). In addition, increased levels of wild-type Rad52 foci caused by the splice variant equivalents may indicate increased DNA damage. However, it is unclear how increased damage could cause a specific preference for repair from the same or a sister chromosome. Indeed, DNA damage elevates repair from both sister and homologous chromosomes (13). In addition, elevated Rad52 foci levels in yeast mutants typically indicate delayed or impaired repair processes.

Disruption of the Rad52-Rad51 interaction and its effects on recombination. C-terminal truncations of Rad52 are known to disrupt its interaction with Rad51, thus impairing the formation of Rad51 filaments (19, 26, 37, 39). Such Rad52 C-terminal truncation mutants are complemented by overexpression of *RAD51* (1, 26). Furthermore, disruption of the Rad52-Rad51 interaction in both yeast and mammalian cells channels recombination intermediates to Rad51-independent repair pathways, such as single-strand annealing (SSA) or break-induced replication (33, 43, 51). The dominant recombination phenotype exhibited by the splice variants may be due to disruption of this Rad52-Rad51 interaction. Indeed, we find that the dominant-negative γ-ray sensitive phenotype of Rad52Δ284 is partially rescued by overexpression of the *RAD51* gene (Fig. 9B). In addition, the *rad52Δ284* allele increases pop-out recombination between *leu2* direct repeats that likely occurs by SSA. Together, these data support the notion that Rad51-dependent pathways have been disrupted.

On the surface, expression of all the variants results in increased direct-repeat recombination in both mammalian cells and yeast. However, further analysis of the recombinants in yeast reveals some differences. For example, the shorter *rad52Δ77* variant increases the frequency of gene conversion events in contrast to *rad52Δ284*, which increases pop-out events. In addition, Rad52Δ77 does not colocalize with wild-type Rad52 in DNA repair foci or cause a dominant-negative γ-ray sensitivity phenotype, like Rad52Δ284 does. However, despite these differences, both yeast variants increase wild-type Rad52 focus levels and increase direct-repeat recombination. Thus, we conclude that these variants may disrupt HDR in a similar way and represent a new phenotype for *rad52* N-terminal mutants (28).

***RAD52* variants favor sister chromatid repair.** We show that the *RAD52* splice variants dominantly increase the frequency of direct-repeat recombination from the same or a sister chromosome in both mammalian cells and yeast. In yeast, where we are able to easily measure the frequency of recombination between heteroalleles on homologous chromosomes, the splice variant equivalents lower the frequency of recombination. Rad51-independent repair pathways are also required for interchromosomal but not intrachromosomal repair in yeast (2). Therefore, it is possible that expression of the *RAD52* splice variants in mammalian cells inhibits RAD51-dependent interchromosomal repair of spontaneous lesions, consequently forcing them to be repaired from the sister chromatid. Perhaps expression of *RAD52+intron8* inhibits the activity of RAD51, impairing the homology search ability of the repair complex. This, in turn, may favor the repair of DSBs using the sister chromatid template, which is tethered by cohesin, rather than searching for a homolog (18, 34). Similarly, depletion of p53 also favors intrachromosomal or sister chromatid repair (53), perhaps mediated through the inhibition of RAD51. Recently, differential expression of splice variants of p53 was found in human breast tumors compared to normal breast tissue (7). Similarly, the differential expression of the *RAD52* splice variants in the various cell types, shown in Fig. SA of the supplemental material, may control selective preferences for recombination in different adult tissues.

ACKNOWLEDGMENTS

We thank Scott Hughes for help with preparing mouse samples, Maureen Ward and Arthur Bank for mouse 3T3 cells and tissue culture reagents, and Lorene Rozier for help with the mitotic shake-off technique. Further, we are indebted to Maria Jasin, Jeremy Stark, and

colleagues for providing the mammalian cell reporter system. We also thank David Bentley for help with the preliminary data outlined in Fig. SA of the supplemental material, Bill Friedewald and Shing Lee for advice on binomial statistics, Christine Richardson and members of the Rothstein lab for critical comments on the manuscript, and Larry Chasin for helping us to attempt to define alternative splicing from raw sequence data.

This work was supported by grants from the Eric Greenberg Foundation, Women-at-Risk Breast Cancer Program, the Berrie Diabetes Foundation, and the NIH (NIGMS and NCI). M.S. was supported by an award from the New York Times Company Foundation to the Columbia University summer research program for science teachers.

REFERENCES

1. **Asleson, E. N., R. J. Okagaki, and D. M. Livingston.** 1999. A core activity associated with the N terminus of the yeast *RAD52* protein is revealed by *RAD51* overexpression suppression of C-terminal *rad52* truncation alleles. Genetics **153:**681–692.
2. **Bai, Y., and L. S. Symington.** 1996. A Rad52 homolog is required for *RAD51*-independent mitotic recombination in *Saccharomyces cerevisiae*. Genes Dev. **10:**2025–2037.
3. **Bendixen, C., I. Sunjevaric, R. Bauchwitz, and R. Rothstein.** 1994. Identification of a mouse homologue of the *Saccharomyces cerevisiae* recombination and repair gene, *RAD52*. Genomics **23:**300–303.
4. **Benson, F. E., P. Baumann, and S. C. West.** 1998. Synergistic actions of Rad51 and Rad52 in recombination and DNA repair. Nature **391:**401–404.
5. **Bi, B., N. Rybalchenko, E. I. Golub, and C. M. Radding.** 2004. Human and yeast Rad52 proteins promote DNA strand exchange. Proc. Natl. Acad. Sci. USA **101:**9568–9572.
6. **Boundy-Mills, K. L., and D. M. Livingston.** 1993. A *Saccharomyces cerevisiae RAD52* allele expressing a C-terminal truncation protein: activities and intragenic complementation of missense mutations. Genetics **133:**39–49.
7. **Bourdon, J. C., K. Fernandes, F. Murray-Zmijewski, G. Liu, A. Diot, D. P. Xirodimas, M. K. Saville, and D. P. Lane.** 2005. p53 isoforms can regulate p53 transcriptional activity. Genes Dev. **19:**2122–2137.
8. **Erdeniz, N., U. H. Mortensen, and R. Rothstein.** 1997. Cloning-free PCR-based allele replacement methods. Genome Res. **7:**1174–1183.
9. **Esashi, F., N. Christ, J. Gannon, Y. Liu, T. Hunt, M. Jasin, and S. C. West.** 2005. CDK-dependent phosphorylation of BRCA2 as a regulatory mechanism for recombinational repair. Nature **434:**598–604.
10. **Fujimori, A., S. Tachiiri, E. Sonoda, L. H. Thompson, P. K. Dhar, M. Hiraoka, S. Takeda, Y. Zhang, M. Reth, and M. Takata.** 2001. Rad52 partially substitutes for the Rad51 paralog XRCC3 in maintaining chromosomal integrity in vertebrate cells. EMBO J. **20:**5513–5520.
11. **Griffin, C. S., and J. Thacker.** 2004. The role of homologous recombination repair in the formation of chromosome aberrations. Cytogenet. Genome Res. **104:**21–27.
12. **Huang, K. N., and L. S. Symington.** 1994. Mutation of the gene encoding protein kinase C 1 stimulates mitotic recombination in *Saccharomyces cerevisiae*. Mol. Cell. Biol. **14:**6039–6045.
13. **Kadyk, L. C., and L. H. Hartwell.** 1992. Sister chromatids are preferred over homologs as substrates for recombinational repair in *Saccharomyces cerevisiae*. Genetics **132:**387–402.
14. **Kagawa, W., H. Kurumizaka, S. Ikawa, S. Yokoyama, and T. Shibata.** 2001. Homologous pairing promoted by the human Rad52 protein. J. Biol. Chem. **276:**35201–35208.
15. **Kagawa, W., H. Kurumizaka, R. Ishitani, S. Fukai, O. Nureki, T. Shibata, and S. Yokoyama.** 2002. Crystal structure of the homologous-pairing domain from the human Rad52 recombinase in the undecameric form. Mol. Cell **10:**359–371.
16. **Kito, K., H. Wada, E. T. Yeh, and T. Kamitani.** 1999. Identification of novel isoforms of human RAD52. Biochim. Biophys. Acta **1489:**303–314.
17. **Klein, H. L.** 1995. Genetic control of intrachromosomal recombination. Bioessays **17:**147–159.
18. **Kobayashi, T., T. Horiuchi, P. Tongaonkar, L. Vu, and M. Nomura.** 2004. *SIR2* regulates recombination between different rDNA repeats, but not recombination within individual rRNA genes in yeast. Cell **117:**441–453.
19. **Krejci, L., B. Song, W. Bussen, R. Rothstein, U. H. Mortensen, and P. Sung.** 2002. Interaction with Rad51 is indispensable for recombination mediator function of Rad52. J. Biol. Chem. **277:**40132–40141.
20. **Krogh, B. O., and L. S. Symington.** 2004. Recombination proteins in yeast. Annu. Rev. Genet. **38:**233–271.
21. **Kumar, J. K., and R. C. Gupta.** 2004. Strand exchange activity of human recombination protein Rad52. Proc. Natl. Acad. Sci. USA **101:**9562–9567.
22. **Lea, D. E., and C. A. Coulson.** 1949. The distribution of the numbers of mutants in bacterial populations. J. Genet. **138:**253–261.
23. **Lisby, M., J. H. Barlow, R. C. Burgess, and R. Rothstein.** 2004. Choreography of the DNA damage response: spatiotemporal relationships among checkpoint and repair proteins. Cell **118:**699–713.
24. **Lisby, M., U. H. Mortensen, and R. Rothstein.** 2003. Colocalization of multiple DNA double-strand breaks at a single Rad52 repair centre. Nat. Cell Biol. **5:**572–577.
25. **Lisby, M., R. Rothstein, and U. H. Mortensen.** 2001. Rad52 forms DNA repair and recombination centers during S phase. Proc. Natl. Acad. Sci. USA **98:**8276–8282.
26. **Milne, G. T., and D. T. Weaver.** 1993. Dominant negative alleles of *RAD52* reveal a DNA repair/recombination complex including Rad51 and Rad52. Genes Dev. **7:**1755–1765.
27. **Mortensen, U. H., C. Bendixen, I. Sunjevaric, and R. Rothstein.** 1996. DNA strand annealing is promoted by the yeast Rad52 protein. Proc. Natl. Acad. Sci. USA **93:**10729–10734.
28. **Mortensen, U. H., N. Erdeniz, Q. Feng, and R. Rothstein.** 2002. A molecular genetic dissection of the evolutionarily conserved N terminus of yeast Rad52. Genetics **161:**549–562.
29. **New, J. H., T. Sugiyama, E. Zaitseva, and S. C. Kowalczykowski.** 1998. Rad52 protein stimulates DNA strand exchange by Rad51 and replication protein A. Nature **391:**407–410.
30. **Paques, F., and J. E. Haber.** 1999. Multiple pathways of recombination induced by double-strand breaks in *Saccharomyces cerevisiae*. Microbiol. Mol. Biol. Rev. **63:**349–404.
31. **Pierce, A. J., R. D. Johnson, L. H. Thompson, and M. Jasin.** 1999. *XRCC3* promotes homology-directed repair of DNA damage in mammalian cells. Genes Dev. **13:**2633–2638.
32. **Raderschall, E., E. I. Golub, and T. Haaf.** 1999. Nuclear foci of mammalian recombination proteins are located at single-stranded DNA regions formed after DNA damage. Proc. Natl. Acad. Sci. USA **96:**1921–1926.
33. **Rattray, A. J., and L. S. Symington.** 1994. Use of a chromosomal inverted repeat to demonstrate that the *RAD51* and *RAD52* genes of *Saccharomyces cerevisiae* have different roles in mitotic recombination. Genetics **138:**587–595.
34. **Reid, R. J., and R. Rothstein.** 2004. Stay close to your sister. Mol. Cell **14:**418–420.
35. **Rijkers, T., J. Van Den Ouweland, B. Morolli, A. G. Rolink, W. M. Baarends, P. P. Van Sloun, P. H. Lohman, and A. Pastink.** 1998. Targeted inactivation of mouse *RAD52* reduces homologous recombination but not resistance to ionizing radiation. Mol. Cell. Biol. **18:**6423–6429.
36. **Rose, M., F. Winston, and P. Hieter.** 1990. Methods in yeast genetics: a laboratory course manual. Cold Spring Harbor Laboratory Press, New York, N.Y.
37. **Shen, Z., K. G. Cloud, D. J. Chen, and M. S. Park.** 1996. Specific interactions between the human RAD51 and RAD52 proteins. J. Biol. Chem. **271:**148–152.
38. **Shin, D. S., L. Pellegrini, D. S. Daniels, B. Yelent, L. Craig, D. Bates, D. S. Yu, M. K. Shivji, C. Hitomi, A. S. Arvai, N. Volkmann, H. Tsuruta, T. L. Blundell, A. R. Venkitaraman, and J. A. Tainer.** 2003. Full-length archaeal Rad51 structure and mutants: mechanisms for RAD51 assembly and control by BRCA2. EMBO J. **22:**4566–4576.
39. **Shinohara, A., and T. Ogawa.** 1998. Stimulation by Rad52 of yeast Rad51-mediated recombination. Nature **391:**404–407.
40. **Singleton, M. R., L. M. Wentzell, Y. Liu, S. C. West, and D. B. Wigley.** 2002. Structure of the single-strand annealing domain of human RAD52 protein. Proc. Natl. Acad. Sci. USA **99:**13492–13497.
41. **Smith, J., and R. Rothstein.** 1999. An allele of *RFA1* suppresses *RAD52*-dependent double-strand break repair in *Saccharomyces cerevisiae*. Genetics **151:**447–458.
42. **Sonoda, E., M. Takata, Y. M. Yamashita, C. Morrison, and S. Takeda.** 2001. Homologous DNA recombination in vertebrate cells. Proc. Natl. Acad. Sci. USA **98:**8388–8394.
43. **Stark, J. M., A. J. Pierce, J. Oh, A. Pastink, and M. Jasin.** 2004. Genetic steps of mammalian homologous repair with distinct mutagenic consequences. Mol. Cell. Biol. **24:**9305–9316.
44. **Stasiak, A. Z., E. Larquet, A. Stasiak, S. Muller, A. Engel, E. Van Dyck, S. C. West, and E. H. Egelman.** 2000. The human Rad52 protein exists as a heptameric ring. Curr. Biol. **10:**337–340.
45. **Sung, P.** 1997. Function of yeast Rad52 protein as a mediator between replication protein A and the Rad51 recombinase. J. Biol. Chem. **272:**28194–28197.
46. **Symington, L. S.** 2002. Role of *RAD52* epistasis group genes in homologous recombination and double-strand break repair. Microbiol. Mol. Biol. Rev. **66:**630–670.
47. **Thomas, B. J., and R. Rothstein.** 1989. Elevated recombination rates in transcriptionally active DNA. Cell **56:**619–630.
48. **Thompson, L. H., and D. Schild.** 2002. Recombinational DNA repair and human disease. Mutat. Res. **509:**49–78.
49. **Thorpe, P. H., B. J. Stevenson, and D. J. Porteous.** 2002. Functional correction of episomal mutations with short DNA fragments and RNA-DNA oligonucleotides. J. Gene Med. **4:**195–204.
50. **Treuner, K., R. Helton, and C. Barlow.** 2004. Loss of Rad52 partially rescues

tumorigenesis and T-cell maturation in Atm-deficient mice. Oncogene **23:** 4655–4661.

51. **Tsukamoto, M., K. Yamashita, T. Miyazaki, M. Shinohara, and A. Shinohara.** 2003. The N-terminal DNA-binding domain of Rad52 promotes *RAD51*-independent recombination in *Saccharomyces cerevisiae*. Genetics **165:**1703–1715.
52. **van den Bosch, M., P. H. Lohman, and A. Pastink.** 2002. DNA double-strand break repair by homologous recombination. Biol. Chem. **383:**873–892.
53. **Yun, S., A. C. C. Lie, and A. C. Porter.** 2004. Discriminatory suppression of homologous recombination by p53. Nucleic Acids Res. **32:**6479–6489.
54. **Zou, H., and R. Rothstein.** 1997. Holliday junctions accumulate in replication mutants via a RecA homolog-independent mechanism. Cell **90:**87–96.